

# Direct growth of ordered N-doped carbon nanotube arrays on carbon fiber cloth as a free-standing and binder-free air electrode for flexible quasi-solid-state rechargeable Zn-Air batteries

Qian Lu<sup>1</sup> | Xiaohong Zou<sup>1</sup> | Kaiming Liao<sup>1</sup> | Ran Ran<sup>1</sup> | Wei Zhou<sup>1</sup> | Meng Ni<sup>2</sup> | Zongping Shao<sup>1,3</sup> 

<sup>1</sup>State Key Laboratory of Materials-Oriented Chemical Engineering, College of Chemical Engineering, Nanjing Tech University, Nanjing, China

<sup>2</sup>Department of Building and Real Estate, The Hong Kong Polytechnic University, Kowloon, Hong Kong, China

<sup>3</sup>WA School of Mines: Minerals, Energy and Chemical Engineering (WASM-MECE), Curtin University, Perth, Western Australia, Australia

## Correspondence

Kaiming Liao and Zongping Shao, State Key Laboratory of Materials-Oriented Chemical Engineering, College of Chemical Engineering, Nanjing Tech University, No. 5 Xin Mofan Road, 210009 Nanjing, China.

Email: [kaimingliao@njtech.edu.cn](mailto:kaimingliao@njtech.edu.cn) (KL) and [shaozp@njtech.edu.cn](mailto:shaozp@njtech.edu.cn) (ZS)

## Funding information

National Natural Science Foundation of China, Grant/Award Number: 51802152; National Key R&D Program of China, Grant/Award Number: 2018YFB0905400; Natural Science Foundation of Jiangsu Province of China, Grant/Award Number: BK20170974

## Abstract

The development of an air electrode that is flexible in physical property and highly active and durable at different geometric status for both oxygen reduction reaction (ORR) and oxygen evolution reaction (OER) is of crucial importance for the rational design of flexible rechargeable Zn-air batteries (ZABs). Considering their good elasticity, high conductivity, and superior thermal and chemical stability, carbon nanotubes have been widely used as a catalyst support in various electrocatalysts, while oxide or metal nanoparticles have been frequently deposited on the carbon nanotube substrate to perform as the active materials. Considering the poor contact between active materials and carbon nanotubes may introduce a challenge for long-term operating stability, in particular in flexible devices, pure carbon electrocatalyst is highly appreciated. Herein, a free-standing air electrode with cobalt nanoparticles encapsulated N-codoped carbon nanotube arrays uniformly grown on the surface of carbon fiber cloth is developed by a two-step in situ growth method. Such a carbon-based electrode shows outstanding activity for both ORR and OER. The flexible ZAB with such air electrode shows superior flexibility and stability working under extreme bending conditions. Moreover, the polarization and round-trip efficiency for the flexible battery is 0.67 V and 64.4% at 2 mA/cm<sup>2</sup>, respectively, even after being operated for 30 hours. This study provides a feasible way to design all carbon-based free-standing and flexible electrode and enlightens the electrode design for flexible energy conversion/storage devices.

## KEYWORDS

carbon nanotube arrays, flexible Zn-air battery, N-doped carbon, quasi-solid-state battery

[The copyright line for this article was changed on June 26, 2021 after original online publication]

This is an open access article under the terms of the Creative Commons Attribution License, which permits use, distribution and reproduction in any medium, provided the original work is properly cited.

© 2020 The Authors. *Carbon Energy* published by Wenzhou University and John Wiley & Sons Australia, Ltd.

## 1 | INTRODUCTION

Rechargeable metal-air batteries, such as Zn-air batteries (ZABs) and Li-air/O<sub>2</sub> batteries,<sup>1-3</sup> have been regarded as next generation of electrochemical energy storage systems/power sources with much higher energy density as compared to state-of-the-art lithium-ion batteries.<sup>4-6</sup> ZABs, which generate electricity through the electrochemical reaction between metallic Zn from the anode and molecular oxygen from ambient air, is of particular interests because of abundant raw materials and aqueous electrolyte that make them more competitive with Li-air batteries from the aspects of cost and safety.<sup>7-9</sup> Recently, flexible ZABs have received increasing attention as power source for wearable devices because of their high energy density, high safety, low cost, and environmental friendliness.<sup>10,11</sup> However, the performance of ZABs is strongly related to air electrode, in which oxygen reduction reaction (ORR) and oxygen evolution reaction (OER) happens during discharge and charge, respectively. The oxygen activation is usually difficult, and many air electrodes suffer from sluggish reaction kinetics for ORR, OER, or both of them, which could result in low round-trip efficiency and poor performance of ZABs.<sup>1,12</sup> Therefore, the development of a bifunctional electrocatalyst that shows high activity for both ORR and OER is key in the development of ZABs, yet a big challenge, in particular for flexible ZABs.

For conventional air electrode, the catalyst in power form is usually deposited on a gas diffusion layer (usually carbon paper) through spray-coating or drop-casting technique, and some binder is often used to create sufficient binding of the catalyst layer to the carbon paper.<sup>13,14</sup> However, the random stacking or the poor dispersion of the catalyst inevitably results in poor transport of oxygen and electron through the air electrode, which may cause sluggish reaction kinetics.<sup>15</sup> Refer to this point, Zhang's group proposed a liquid-phase chemical method to prepare a NiFe-layer double hydroxide-loaded asymmetric air cathode with internal three-dimensional (3D) multiphase interface, thus allowing oxygen diffusion and electrolyte permeation within the 3D-air electrode,<sup>13</sup> and the ZAB with this 3D-air electrode demonstrated promising cell performance. By rationally designing 3D-air electrode with an ordered structure, the gas permeation within the void space of air electrode and electronic conductivity inside the electrode bulk is greatly facilitated, improved electrode reaction kinetics is then expected.<sup>16,17</sup>

In flexible ZABs, the air electrode frequently experiences geometry deformed situation, thus the air electrode should be flexible as well.<sup>18</sup> Currently, the air electrode for flexible ZABs is usually fabricated by depositing

bifunctional catalysts, such as oxides, metal sulfides, or metals, or a mixture of them, on a 3D flexible substrate such as carbon fiber cloth.<sup>16,19,20</sup> Such bifunctional catalysts are typically rigid, and their contact with the substrate is usually weak. The frequent geometric deforming of the ZABs may lead to the detachment of the electrocatalysts from the surface of the flexible substrate, thus introducing a big concern for long-term operation. As we know, carbon materials are highly conductive, good thermal and chemical stability, and high flexibility in certain structure, for example, carbon nanotubes and graphene.<sup>21,22</sup> It suggests if the catalytic activity of carbon materials for both ORR and OER can be greatly improved, they are superior electrocatalysts for ZABs. Until now, carbonaceous material, such as heteroatom-doped porous carbon, heteroatom-doped carbon nanotube, and heteroatom-doped graphene, have been extensively investigated as promising ORR or OER electrocatalysts with low cost, excellent conductivity, and high surface area.<sup>21,23,24</sup> However, the random piling of carbonaceous materials in electrode inhibits the transport of oxygen and electron, leading to inferior discharge rate capacities. In some studies, activated carbon fiber cloth, prepared by a two-step activation method, with abundant oxygen functional groups was directly applied as a bifunctional air electrode for flexible rechargeable ZABs.<sup>25</sup> Unfortunately, the extremely low surface area of 0.51 m<sup>2</sup>/g was observed for the activated carbon fiber cloth, showing limited catalytic active sites for ORR and OER. In another study, an N and S codoped porous carbon fiber cloth with a surface area of 146.2 m<sup>2</sup>/g was prepared and applied as 3D-air electrodes for flexible rechargeable ZABs by Zhao et al.,<sup>26</sup> unfortunately large charge polarization was still demonstrated in their work.

In general, transition metal and heteroatom-doped carbon materials have shown the evident advantages in both performance and economy.<sup>27,28</sup> For instance, nitrogen-doped porous carbon with embedded cobalt nanoparticle was synthesized by a spontaneous gas-foaming strategy, and a low voltage polarization of 0.73 V at 10 mA/cm<sup>2</sup> was achieved for ZABs by using it as the air electrode.<sup>29</sup> In addition, bimetal FeCo nanoparticles enclosed by N-doped carbon nanotubes were also reported as a cost-effective and efficient bifunctional catalyst.<sup>27</sup> Recently, FeNi@NCNTs deposited on pure carbon fiber cloth was applied as air electrode for flexible rechargeable ZABs.<sup>30</sup> Unfortunately, the randomly stacked FeNi@NCNTs catalysts on carbon fiber cloth caused slow transport of oxygen and electron through the whole electrode, consequently, inferior discharge/charge capacities of batteries were demonstrated. Therefore, it is highly desirable to design a flexible air electrode with a uniform dispersion of nitrogen-doped carbon-based

bifunctional catalysts on carbon fiber cloth in an ordered manner for flexible ZABs.

Herein, we report the direct growth of cobalt, nitrogen-codoped carbon nanotubes (Co-NCNT) arrays on the substrate of carbon fiber cloth in an ordered manner with outstanding ORR and OER bifunctionality and superior flexibility as air electrode of flexible ZABs. Such electrode was facilely synthesized via a two-step procedure including the acid etching of carbon fiber cloth and in situ growth of Co-NCNTs via chemical vapor deposition. The aqueous ZABs with such an air electrode demonstrated better discharge/charge performance than air electrode with unevenly dispersed Co-NCNT on carbon fiber cloth, prepared through conventional spray deposition, and other contrastive air electrodes without Co-NCNT. As a proof of concept, the flexible quasi-solid-state ZABs with such an air electrode showed excellent flexibility during the discharge/charge process. Moreover, the polarization and round-trip efficiency for the flexible

battery are respectively 0.67 V and 64.4% at 2 mA/cm<sup>2</sup> even after continuous operation for 30 hours. The fundamental understanding of the Co-NCNT array formation and the enhanced catalytic performance was further exploited.

## 2 | RESULTS AND DISCUSSION

The uniform growth of N-doped carbon nanotube arrays on active carbon cloth (CC-A) was realized via the chemical vapor deposition process with the synthesis procedure schematically depicted in Figure 1A. For the in situ homogeneous growth of carbon nanotubes on the surface of carbon cloth, the metal catalyst over the substrate surface plays a key role. As mentioned, fresh carbon fiber cloth usually has a low specific surface area. As shown in Figures S1A and S1C, the surface of untreated carbon fiber in carbon cloth is relatively smooth.

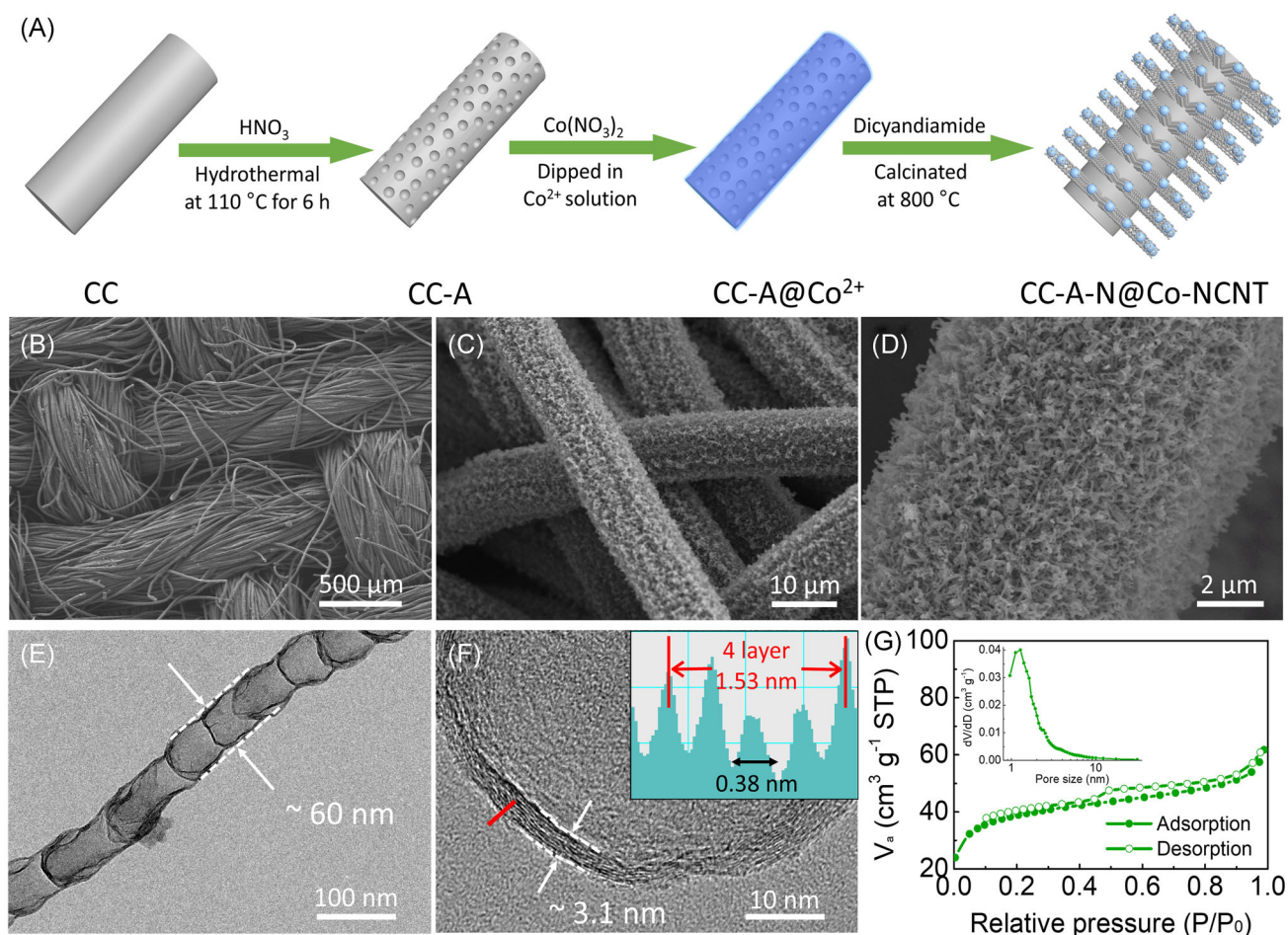


**FIGURE 1** A, Illustrated formation procedures of the CC-A-N@Co-NCNT, scanning electron microscope images of (B-D) CC-A-N@Co-NCNT at different magnification. E, Transmission electron microscopy image of Co-NCNT. F, High-resolution transmission electron microscopy image of Co-NCNT. G, Nitrogen adsorption-desorption isotherm and corresponding pore size distribution of CC-A-N@Co-NCNT

The amount of metal catalyst deposited on the smooth surface of untreated carbon cloth is limited, in addition, such metal catalysts can migrate and aggregate easily during high-temperature treatment, causing uneven distribution of the carbon nanotubes and the abnormal growth of cobalt particles. Therefore, activating carbon cloth with increased surface area to increase the amount of deposited metal catalyst, and abundant surface pores (defects) to increase the homogeneity of metal catalyst distribution and suppress the catalyst migration, is extremely crucial for the even and ordered growth of the carbon nanotubes. Herein, we first activated the pristine carbon fiber cloth with a concentrated nitric acid solution through hydrothermal reaction. Through etching by the strong nitric acid, a lot of surface defects over the carbon surface were introduced, and substantially increased specific surface area of the carbon was realized. From the scanning electron microscope (SEM) images as shown in Figures S1B and S1D, after the treatment, the surface of the carbon fibers (CC-A) became rough, and many pores on the surface of carbon fibers were formed. The pore structure of the treated sample (CC-A) was further analyzed by nitrogen adsorption-desorption isotherm. As shown in Figure S1E, the sharp nitrogen uptake at a low relative pressure region ( $p/p_0 < 0.1$ ) and the obvious hysteresis at a moderate relative pressure region ( $p/p_0 > 0.45$ ) implies the existence of micropore and mesopore, respectively.<sup>31,32</sup> The pore size distribution of CC-A was calculated by Barrett-Joyner-Halenda equation from adsorption curve, showing the overall pore size of smaller than 10 nm and average pore size of about 2.2 nm (Figure S1F). The pore volume was calculated to be  $0.13 \text{ cm}^3/\text{g}$ . The specific surface area was also calculated by the Brunauer-Emmett-Teller equation and turned out to be  $230 \text{ m}^2/\text{g}$ , substantially larger than that of pristine carbon cloth (less than  $1.0 \text{ m}^2/\text{g}$ ). The high specific surface area was mainly introduced from the newly formed pores on the surface of carbon fibers due to the  $\text{HNO}_3$  etching pores. Such pores can serve as the anchoring sites for the fixing of cobalt precursor to greatly improve the cobalt loading and prevent the growth of cobalt nanoparticles at high calcination temperature for the conversion of cobalt precursor to metallic cobalt (Figure S2A). As a proof-of-concept, the CC-A-N@Co with cobalt particles loaded on active carbon cloth was prepared at a temperature of  $800^\circ\text{C}$ . As shown in Figures S2C and S2D, the cobalt nanoparticles, with a particle size of small than 60 nm, are homogeneously dispersed over the carbon fibers, and the pores on the surface of carbon fibers are covered with cobalt nanoparticles.

Two different samples of N-doped carbon nanotubes grown on carbon fiber cloth, that is, CC-A-N@Co-NCNT and CC-N@Co-NCNT, were then prepared by the CVD

method using CC-A (acid-treated carbon cloth) and CC (pristine carbon cloth) as the substrate, respectively. The morphology of the as-prepared CC-A-N@Co-NCNT and CC-N@Co-NCNT samples were first characterized by SEM. As shown in Figures 1B and S3A, the as-prepared CC-A-N@Co-NCNT sample retained the original morphological structure of the carbon cloth after conducting the chemical vapor deposition process, while the surface of compositional carbon fibers was heavily but evenly decorated with nanotubes (Figure 1C). The nanotube arrays, which surrounded the carbon fibers, are more clearly observed from the magnified SEM images as shown in Figure 1D. In addition, according to the cross-sectional SEM image of the carbon fibers in CC-A-N@Co-NCNT as shown in Figure S3B, the thickness of the nanotube array is about  $1 \mu\text{m}$ . In comparison, obvious cobalt particles and bare carbon fibers are observed from the CC-N@Co-NCNT sample (Figure S4). The large cobalt particles, caused by the agglomeration of cobalt precursor during high-temperature calcination, were failed for inducing the growth of carbon nanotubes. In addition, the uneven growth of stacked nanotubes was also obviously observed. The above results clearly demonstrated the significant benefits of acid etching for the direct growth of carbon nanotubes on the carbon cloth. Moreover, the optimal concentration of  $\text{Co}(\text{NO}_3)_2$  solution was also investigated. As shown in Figure S5, the bare carbon fibers and cobalt particles are clearly observed for the CC-A-N@Co-NCNT samples prepared with low ( $0.1 \text{ g/mL}$ ) and high ( $1 \text{ g/mL}$ ) concentration of  $\text{Co}(\text{NO}_3)_2$  solution, respectively. It reveals the concentration of  $0.4 \text{ g/mL}$  as applied in this study is near the optimal value, which was then selected for further exploration.

The transmission electron microscopy image in Figure 1E shows the bamboo-like carbon nanotubes with a diameter of approximately 60 nm, coinciding with the observation of SEM images in Figures S2 and S3C. From the high-resolution transmission electron microscopy image in Figure 1F, a lattice spacing of 0.38 nm was observed for the obtained carbon nanotube which was found to have a wall thickness of about 3.1 nm (approximately 8 carbon layer), demonstrating their multiwall nature. The nitrogen adsorption-desorption isotherm and pore size distribution of CC-A-N@Co-NCNT were measured and calculated with the results shown in Figure 1G. The specific surface area and pore volume are found to be  $140 \text{ m}^2/\text{g}$  and  $0.10 \text{ cm}^3/\text{g}$ , respectively, for the CC-A-N@Co-NCNT. Compared to pure CC-A, the reduced pore volume and specific surface area of CC-A-N@Co-NCNT were mainly attributed to the coverage of surface pore by carbon nanotubes, which further demonstrated the cobalt nanoparticles mainly occupied the pores of carbon fibers.

To analyze the composition of the nanotubes in CC-A-N@Co-NCNT, various characterizations, including X-ray diffraction (XRD), Raman, and X-ray photoelectron spectroscopy (XPS), were conducted. As shown in Figure 2A, the XRD diffraction peaks at  $2\theta$  of  $24.5^\circ$  and  $43.5^\circ$  are assigned to characteristic peaks of graphite carbon for the CC-A-N. For CC-A-N@Co-NCNT, the diffraction peaks at  $2\theta$  of  $44.3^\circ$ ,  $51.6^\circ$ , and  $75.9^\circ$  are the characteristic peaks of metallic cobalt (PDF card No. 01-089-4307),<sup>29</sup> which served as the catalysts for depositing the carbon nanotubes. In addition, a weak diffraction peak at  $2\theta$  of  $26.2^\circ$ , corresponded to (002) plane of the carbon nanotubes, is also observed.<sup>27</sup> According to the Raman spectroscopy, as shown in Figure 2B, three peaks below the wavenumbers of  $800\text{ cm}^{-1}$  are observed, that is, 672, 514, and  $465\text{ cm}^{-1}$ , which are attributed to the characteristic peaks of CoO.<sup>11,33</sup> The peaks at  $1342$  and  $1594\text{ cm}^{-1}$  are attributed to the disordered and graphite carbon respectively, suggesting the presence of carbon in the samples.<sup>18,34</sup> The  $I_D/I_G$  ratio is an indication of the

graphitization degree of the carbon. The lowest value of  $I_D/I_G$  was observed for CC-A-N@Co-NCNT, suggesting the highest graphitization degree of the Co-NCNT among the others.<sup>18</sup>

XPS spectroscopy provides useful information about the surface chemical compositions of the catalysts. From the high-resolution C 1s XPS spectrum in Figure 2C, five peaks with bond energies of 284.6, 285.6, 286.5, 288.2, and 291.4 eV are observed, which can be identified to the C–C, C–N/C–O, C=N/C=O, O=C–O, and  $\pi$ – $\pi^*$ , respectively.<sup>31,35</sup> The presence of C and N bonds in XPS demonstrated nitrogen was successfully incorporated into the structure of carbon nanotubes during the growth of carbon nanotubes via chemical vapor deposition. It was suggested that the ORR activity of carbon materials is greatly affected by the configuration of the C and N bonds in their structure. As shown in Figure 2D, there are three peaks located at 398.6, 400.5, and 401.1 eV, which are attributed to pyridinic-N, pyrrolic-N, and graphitic-N, respectively.<sup>36,37</sup> Specially, the content of pyridinic-N and

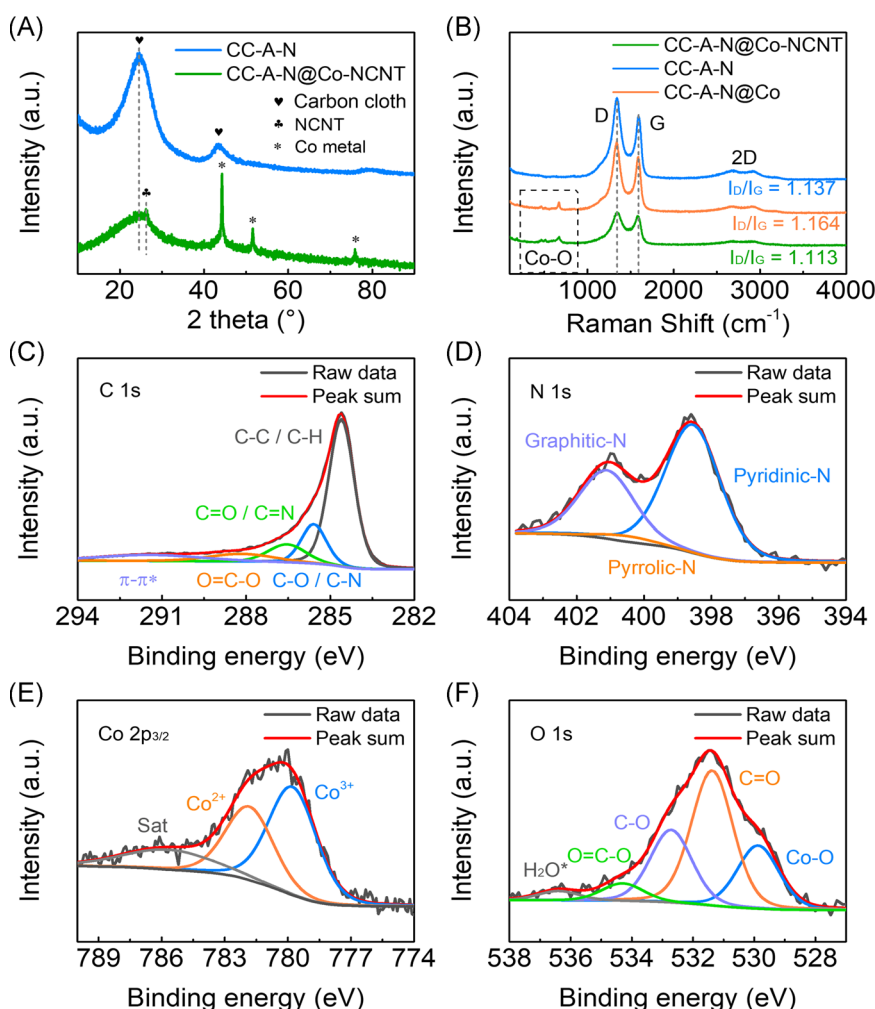


**FIGURE 2** A, X-ray diffraction pattern of the CC-A-N@Co-NCNT and CC-A-N. B, Raman scattering spectra of CC-A-N@Co-NCNT, CC-A-N@Co, and CC-A-N, high-resolution elemental X-ray photoelectron spectra of Co-NCNT: (C) C 1s, (D) N 1s (E) Co 2p, and (F) O 1s

graphitized-N accounts for approximately 97% of the total nitrogen in the structure, which are believed to be the active sites for ORR, thus favorable ORR activity is expected.<sup>38</sup> The high-resolution Co 2p<sub>3/2</sub> spectrum of Co-NCNT is shown in Figure 2E. Three peaks at 779.8, 781.8, and 785.7 eV can be identified as Co<sup>3+</sup>, Co<sup>2+</sup>, and satellite peak of Co<sup>2+</sup>, respectively.<sup>19,39,40</sup> It suggests some surface cobalt was oxidized to CoO<sub>x</sub>. As it is well known that cobalt oxides are good catalyst for OER. Consequently, good bifunctionality with high activity for both ORR and OER is expected for the as-prepared CC-A-N@Co-NNCTs. Interestingly, the signal of cobalt metal was not detected by XPS although the cobalt metal is presented at a noticeable amount in the sample based on XRD. As we know that the detection depth of XPS is only about 5 nm, and the thickness of the carbon wall is about 3.1 nm. It reveals that the encapsulated cobalt metal, inside carbon nanotubes, was likely cladded by a thin cobalt oxide layer. To further confirm the formation of C-O and Co-O bonds, the high-resolution O 1s spectrum was analyzed in Figure 2F. The O 1s spectrum can be deconvoluted into five peaks located at 529.9, 531.4, 532.7, 534.3, and 536.4 eV, which are assigned to Co-O, C=O, C-O, O=C-O, and H<sub>2</sub>O\*, respectively.<sup>25,31,41</sup> In addition, the atomic and mass contents of C, N, O, and Co were listed in Table S1. It was demonstrated that the surface oxygen-contained groups are highly active for ORR and OER. It will further contribute to good bifunctionality of the catalyst.<sup>25,42,43</sup>

The catalytic activity of the as-grown Co-NCT was then first investigated by rotation speed electrode in 0.1M KOH solution based on three-electrode configuration, and the test was conducted by using a powder-form catalyst. According to Figure S6A, the typical linear sweep voltammetry (LSV) curves of ORR for both Co-NCNT and Pt/C catalysts were exhibited. The prepared Co-NCNT catalyst showed excellent ORR electrocatalytic activities with the half-wave potential of 0.805 V, which approached the commercial Pt/C catalysts with a half-wave potential of 0.830 V. In addition, the limited current densities of Co-NCNT and Pt/C catalysts are both improved with the increase of rotating speed, confirming diffusion-limited for the ORR process (Figure S6B,C). Based on Koutecky-Levich equation, the calculated electron transfer number (*n*) for Co-NCNT and Pt/C are 3.6 and 4.0, respectively, demonstrating the four electron reduction pathway for the ORR process (Figure S6D). Furthermore, the typical LSV curves of OER for Co-NCNT and RuO<sub>2</sub> catalysts are exhibited in Figure S6E. The over potential at a current density of 10 mA/cm<sup>2</sup> for the Co-NCNT catalyst is 1.63 V, which is only slightly lower than the commercial RuO<sub>2</sub> catalysts with 1.59 V (Figure S6E), showing the excellent OER performance for the Co-NCNT catalyst. As shown in Figure S6F, the Co-NCNT catalyst showed the potential gap of 0.83 V

between the half-wave potential for ORR and potential at 10 mA/cm<sup>2</sup> for OER, implying the Co-NCNT catalyst is a potential bifunctional oxygen electrocatalyst.<sup>44,45</sup>

To test the performance of the as-prepared CC-A-N@Co-NNCTs in rechargeable ZABs, a ZAB with the material as self-standing air electrode, zinc foil as the anode, and a 6M KOH and 0.2M ZnCl<sub>2</sub> mixed aqueous solution as the electrolyte was constructed (Figure 3A). The discharge performance of the ZABs was first explored, and comparison was made with similar cells of different air electrodes. As shown in Figure S7A, the discharge voltages at 100 mA/cm<sup>2</sup> are 1.07, 0.87, 0.7, 0.67, and 0.41 V for the ZABs with CC-A-N@Co-NCNT, CC-A-N, CC-A, CC-A-N@Co, and CC as the air electrodes, respectively. The ZAB with the CC-A-N@Co-NCNT air electrode also showed the highest power density of 172 mW/cm<sup>2</sup> as compared with that of other air electrodes with 118, 84, 68, and 41 mW/cm<sup>2</sup>, respectively as described above. In addition, the discharge voltages of the ZAB with the CC-A-N@Co-NCNT air electrode at current densities of 5 mA/cm<sup>2</sup> for 20 hours and 10, 20, 30, 40 and 50 mA/cm<sup>2</sup> for 1 hour are obviously higher than those of the ZABs with other contrastive electrodes without growing the Co-NCNT (Figure S7B,C). These results demonstrate that the best performance of Co-NCNT for ORR. According to Figure 3B, a rapid drop of voltage is observed for the ZAB with the CC-N@Co-NCNT air electrode if the discharge current is higher than 90 mA/cm<sup>2</sup>. More importantly, the maximum power density of the ZABs with the CC-A-N@Co-NCNT air electrode is 172 mW/cm<sup>2</sup>, which surpasses that of 129 mW/cm<sup>2</sup> for the ZAB with the CC-N@Co-NCNT air electrode. The ZAB with the CC-A-N@Co-NCNT air electrode demonstrated a stable discharge platform of 1.29 V at 5 mA/cm<sup>2</sup> for 20 hours. As a comparison, the ZAB with the CC-N@Co-NCNT cathode demonstrated a similar discharge voltage of 1.28 V (Figure S8). However, with the increase of polarization current density, the ZAB with the CC-N@Co-NCNT electrode demonstrated much better performance. For example, the discharge voltages of the ZAB with the CC-A-N@Co-NCNT air electrode are 1.27, 1.23, 1.20, 1.17, and 1.13 V at 10, 20, 30, 40 and 50 mA/cm<sup>2</sup>, respectively, while that of the ZAB with the CC-N@Co-NCNT air electrode only 1.25, 1.17, 1.07, 1.00, and 0.94 V correspondingly (Figure 3C). The improved discharge performance at higher current density demonstrated that the ordered Co-NCNT array (CC-A-N@Co-NCNT) facilitated the mass transfer (for oxygen) as compared to the disordered Co-NCNT electrode (CC-N@Co-NCNT), thus the concentration polarization was effectively reduced.

The charge performance of a ZAB is closely related to the OER activity of its air electrode. As shown in Figure

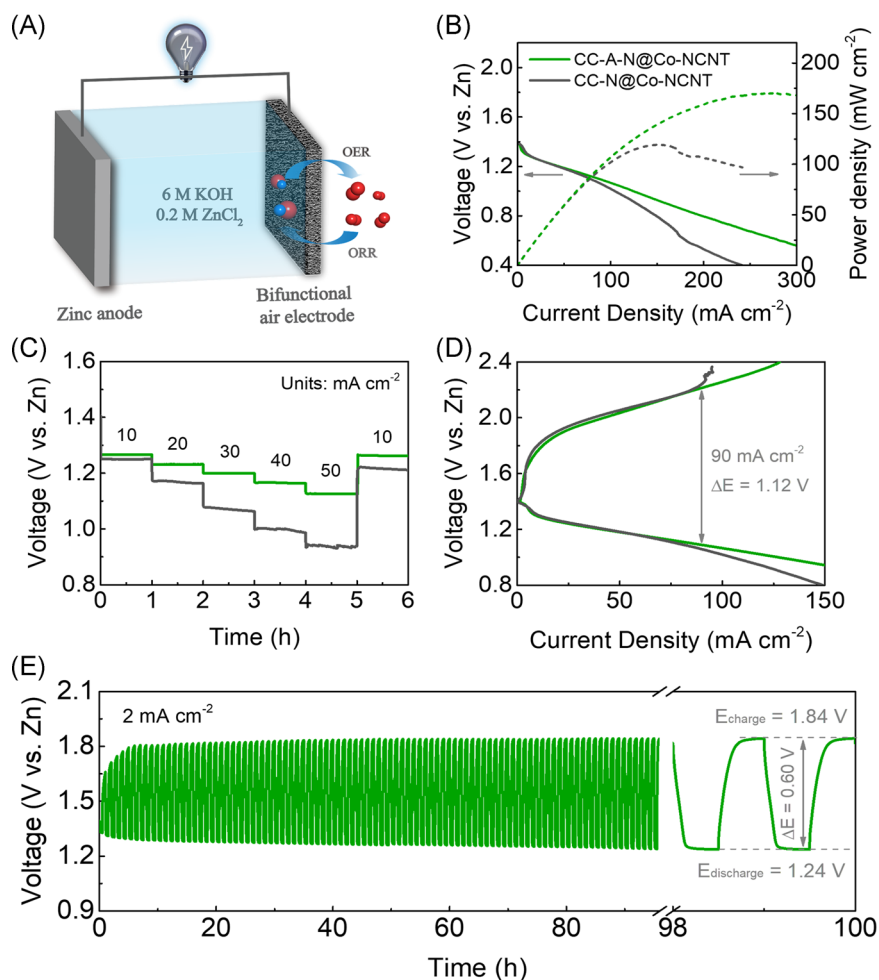


**FIGURE 3** A, Diagram of zinc-air battery, (B) polarization (V-j) curves and power density (P-j) curves, (C) galvanostatic discharge test at different current density of 10 to 50 mA/cm<sup>2</sup> for 1 hour, (D) discharge/charge polarization curves, (E) galvanostatic charge/discharge test for the Zn-air batteries with CC-A-N@Co-NCNT cathode

S7D, the current densities are 42.2, 29.9, 22.6, 14.1, and 0.7 mA/cm<sup>2</sup> at a voltage of 2.0 V (vs Zn) for the ZABs with the CC-A-N@Co-NCNT, CC-A-N, CC-A, CC-A-N@Co, and CC air electrodes, respectively. It suggests the CC-A-N@Co-NCNT electrode also had the best performance for OER among the various electrodes, agreeing well with the previous three-electrode test. Similar charge performance was observed for the ZABs with the CC-A-N@Co-NCNT and CC-N@Co-NCNT electrodes at a current density of lower than 90 mA/cm<sup>2</sup> (Figure 3D). However, the ZAB with the CC-A-N@Co-NCNT electrode showed much better performance than the ZAB with the CC-N@Co-NCNT electrode at polarization current density of higher than 90 mA/cm<sup>2</sup>, revealing the generated oxygen bubble could not flee freely from the electrode at high current density for the disorder electrode (CC-N@Co-NCNT). According to the galvanostatic charge/discharge test, as shown in Figure S7E, the ZAB with the CC-A-N@Co-NCNT air electrode exhibited the best cycling performance compared to the similar ZABs with other

contrastive electrodes. As shown in Figures 3E and S9, the charge/discharge polarization and round-trip efficiency of the ZAB with the CC-A-N@Co-NCNT air electrode are respectively 0.60 V and 67.4% at 2 mA/cm<sup>2</sup> after continuous operation for 100 hours, while that of the ZAB with the CC-N@Co-NCNT air electrode are only 0.73 V and 62.7%. The cycling performance at 5 mA/cm<sup>2</sup> was also explored for the ZAB with the CC-N@Co-NCNT air electrode. As shown in Figure S10, the charge/discharge polarization and round-trip efficiency are respectively 0.67 V and 65.1% at 5 mA/cm<sup>2</sup> after the continuous operation for 50 hours. Considering the same active species of Co-NCNT in both the CC-A-N@Co-NCNT and CC-N@Co-NCNT electrodes, the better performance of the ZAB with the ordered CC-A-N@Co-NCNT air electrode, including higher power density, is a result of the optimized electrode microstructure.

Based on the above-mentioned analysis, the proposed mechanism of ORR/OER (discharge/charge) for the CC-A-N@Co-NCNT and CC-N@Co-NCNT electrodes are

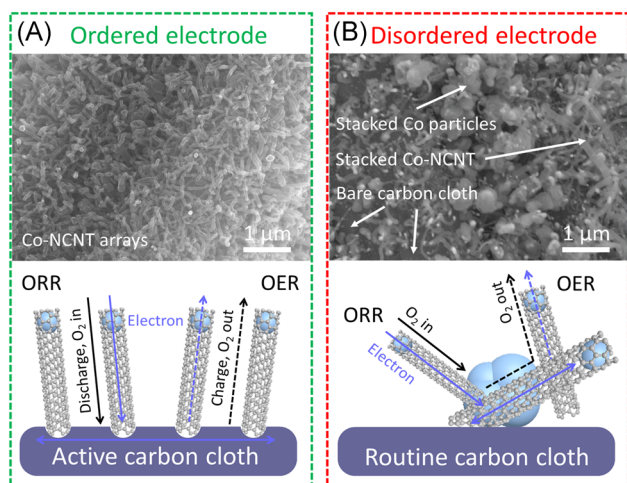


**FIGURE 4** The mechanism of oxygen reduction reaction/oxygen evolution reaction (ORR/OER) (discharge/charge) for the (A) CC-A-N@Co-NCNT, and (B) CC-N@Co-NCNT electrode

presented in Figure 4. For the ordered electrode of CC-A-N@Co-NCNT with the vertical dispersion of Co-NCNT array (Figure 4A), during the discharge process, oxygen can easily access to the whole electrode with optimal diffusion path, thus improving the oxygen reduction kinetics. For the charge process, the generated oxygen bubbles can be effectively removed from the surface of the Co-NCNT active sites to the outside of the ordered air electrode because of the easy gas diffusion as well.<sup>20,46</sup> In addition, the generated electron can directly flow from the Co-NCNT to carbon fiber with the minimized conducting distance. For the disordered air electrode (CC-N@Co-NCNT), the diffusion route of the oxygen bubble was inhibited by the stacked Co-NCNT and large cobalt particles during the OER (discharge) process (Figure 4B). As a result, the generated oxygen bubbles could not remove from the electrode easily at high current density, causing concentration polarization resistance. As shown in Figure 3D, the ZABs with the CC-N@Co-NCNT air electrode showed fast performance degradation if the polarization current density exceeded 90 mA/cm<sup>2</sup>. In addition, owing to the randomly stacked Co-NCNT, poor contact between individual carbon nanotubes would decrease the apparent conductivity of the electrode, leading to poor rate performance of ZABs.

Considering the excellent flexibility of CC-A-N@Co-NCNT, its use as the air electrode of flexible ZABs was further exploited. As shown in Figure 5A, an alkaline gel polymer electrolyte (separator) was sandwiched between the CC-A-N@Co-NCNT pasted on nickel foam (cathode) electrode and zinc foil (anode) electrode. A digital photograph of the assembled flexible ZABs, with an open circuit voltage of 1.42 V, was shown in Figure 5B.

The low discharge/charge polarization for the flexible battery was also observed in Figure 5C, and the power density of the flexible ZAB reached 44 mW/cm<sup>2</sup> at a high current density of 40 mA/cm<sup>2</sup>. Moreover, the flexible ZABs with the CC-A-N@Co-NCNT air electrode delivered a stable discharge platform of 1.25 V at 2 mA/cm<sup>2</sup> for 3 hours, reflecting the excellent stability of the electrode during discharge process (Figure 5D). To evaluate the flexibility, the ZABs with the CC-A-N@Co-NCNT air electrode was evaluated at 2 mA/cm<sup>2</sup> for 20 minutes per cycle under different bending conditions (0°, 90°, and 180°). Under the pristine and other bending conditions, almost the same discharge/charge curves are observed (Figure 5E), highlighting the excellent flexibility of the ZABs. The corresponding digital photographs of the flexible batteries under different bending conditions are presented in Figure 5F. The cycling stability of the flexible battery was further evaluated by a galvanostatic discharge/charge test at 2 mA/cm<sup>2</sup>. As shown in Figure 5G, the flexible ZAB demonstrated excellent cycling stability with only a slight polarization voltage increase after the continuous operation for 30 hours. More importantly, the charge/discharge polarization and round-trip efficiency for the flexible ZAB still reached respectively 0.67 V and 64.4% at 2 mA/cm<sup>2</sup> after the operation for 30 hours. A comparison between our work with the previous reports from the literature of flexible ZABs is conducted with the results listed in Table S2, which further emphasizes the superiority of our flexible electrode. Finally, to demonstrate its great potential as practical flexible power sources for flexible electronic devices, three flexible ZABs are connected in series which successfully powered an LED viewing screen under flat and bending condition, as shown in Figure 5H.

### 3 | CONCLUSION

In summary, an ordered electrode with N-doped carbon nanotube arrays direct grown on carbon fiber cloth was successfully prepared by a two-step synthesis procedure involving acid-etching pretreatment of the carbon cloth and chemical vapor deposition of the N-doped CNT array. This composite electrode exhibited remarkable electrolysis bifunctionality for both ORR and OER. The ZABs assembled from such array architecture electrodes showed enhanced electrochemical performances, including high power density, low polarization, high discharge voltages, and high round-trip efficiency, compared to that of other carbon fiber-based air electrodes. In addition, the combination of the ordered N-doped carbon nanotube arrays and the free-standing carbon fiber cloth substrate allowed fast transport of

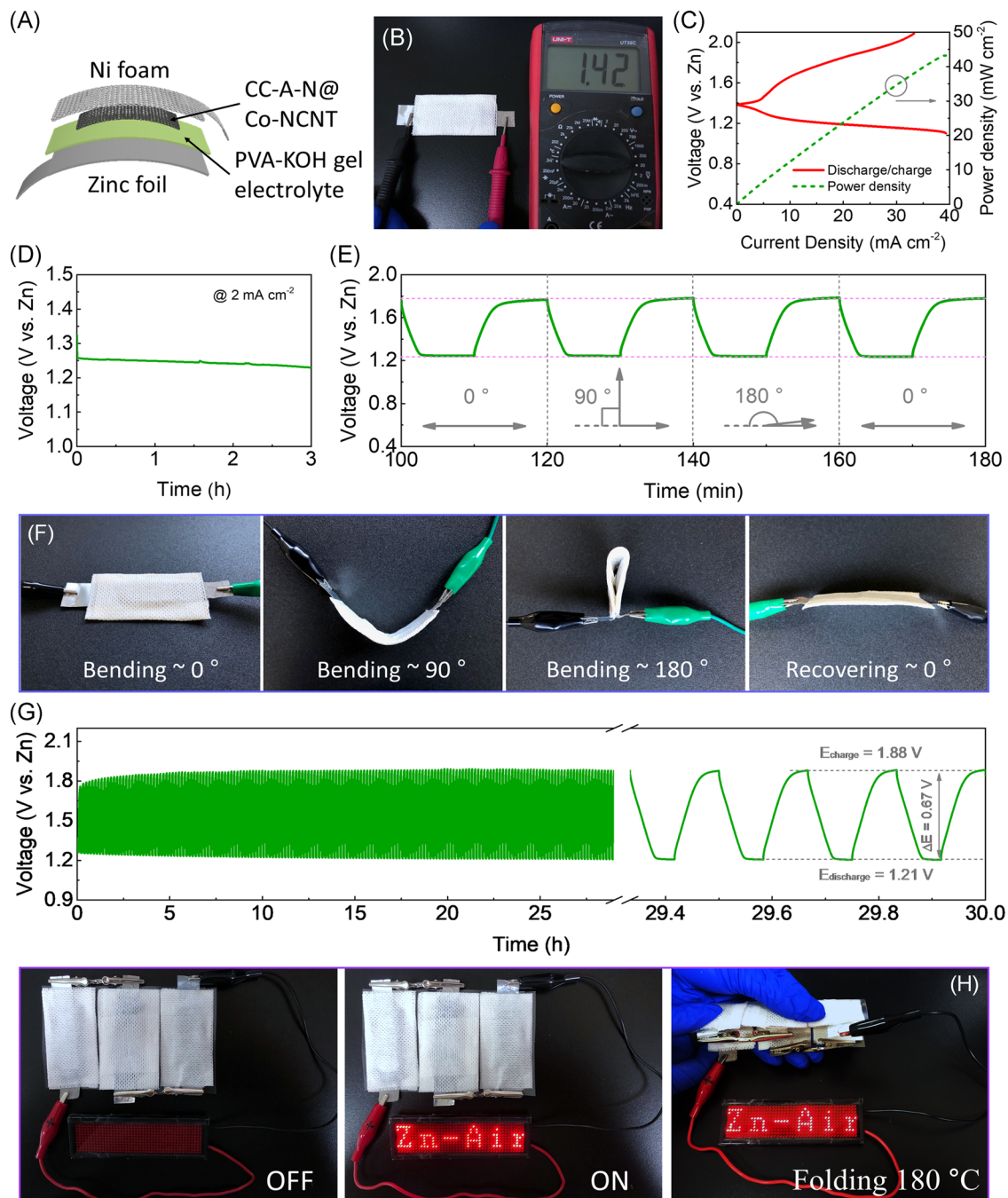


**FIGURE 5** A, Diagram of the flexible solid Zn-air batteries. B, Photograph of the flexible battery with an open circuit voltage of 1.42 V. C, Discharge/charge polarization and power density (P-j) curves of flexible battery. D, Galvanostatic discharge test at 2 mA/cm<sup>2</sup> for 3 hours. E, Discharging/charging curve under different bending conditions at 2 mA/cm<sup>2</sup> (20 minutes for each cycle). F, Photograph of the flexible battery bending at 0°, 90°, 180°, and 0°. G, Galvanostatic charge/discharge test at 2 mA/cm<sup>2</sup> for 30 hours, and (H) three tandem flexible solid batteries used to lighten a LED screen under different bending conditions

oxygen and electron throughout the whole electrode, thus resulting in better cycling performance and rate capability compared with the disordered Co, N-codoped carbon nanotube air electrode. As a result, quasi-solid-state ZABs with such cathode exhibited superb flexibility and delivered a power density of 44 mW/cm<sup>2</sup> even at a

high current density of 40 mA/cm<sup>2</sup>. Moreover, the flexible battery also exhibited good cycling stability. After cycling at 2 mA/cm<sup>2</sup> for 30 hours, a low charge/discharge polarization of 0.67 V, and a high round-trip efficiency of 64.4% was still achieved, holding great potential in the implementation of flexible quasi-solid-state ZABs.

Moreover, the designed electrode is also instructive in many potential flexible energy devices, such as supercapacitor and Li-air/Li-S batteries.

## ACKNOWLEDGMENTS

Zongping Shao and Kaiming Liao thank the funding support provide by the National Key R&D Program of China (Grant no. 2018YFB0905400). Kaiming Liao thanks the funding support provided by the National Natural Science Foundation of China (Grant no. 51802152) and the Natural Science Foundation of Jiangsu Province of China (Grant no. BK20170974). A Project Funded by Priority Academic Program Development of Jiangsu Higher Education Institutions.

## ORCID

Zongping Shao  <http://orcid.org/0000-0002-4538-4218>

## REFERENCES

- Li Y, Dai H. Recent advances in zinc-air batteries. *Chem Soc Rev.* 2014;43(15):5257-5275.
- Zou X, Liao K, Wang D, et al. Water-proof, electrolyte-novolatile, and flexible Li-Air batteries via O<sub>2</sub>-Permeable silica-aerogel-reinforced polydimethylsiloxane external membranes. *Energy Storage Mater.* 2020;27:297-306.
- Lee J-S, Tai Kim S, Cao R, et al. Metal-air batteries with high energy density: Li-air versus Zn-air. *Adv Energy Mater.* 2011; 1(1):34-50.
- Chu S, Cui Y, Liu N. The path towards sustainable energy. *Nat Mater.* 2016;16(1):16-22.
- Zhou S, Fang C, Song X, Liu G. The influence of compact and ordered carbon coating on solid-state behaviors of silicon during electrochemical processes. *Carbon Energy.* 2020;2(1): 143-150.
- Lu Q, Zou X, Ran R, Zhou W, Liao K, Shao Z. An "electro-negative" bifunctional coating layer: simultaneous regulation of polysulfide and Li-ion adsorption sites for long-cycling and "dendrite-free" Li-S batteries. *J Mater Chem A.* 2019;7(39): 22463-22474.
- Zhong Y, Xu X, Wang W, Shao Z. Recent advances in metal-organic framework derivatives as oxygen catalysts for zinc-air batteries. *Batteries Supercaps.* 2018;2(4):272-289.
- Meng X, Liao K, Dai J, et al. Ultralong cycle life Li-O<sub>2</sub> battery enabled by a MOF-derived ruthenium-carbon composite catalyst with a durable regenerative surface. *ACS Appl Mater Interfaces.* 2019;11(22):20091-20097.
- Zou X, Lu Q, Zhong Y, Liao K, Zhou W, Shao Z. Flexible, flame-resistant, and dendrite-impermeable gel-polymer electrolyte for Li-O<sub>2</sub>/air batteries workable under hurdle conditions. *Small.* 2018;14(34):1801798.
- Tan P, Chen B, Xu H, et al. Flexible Zn- and Li-air batteries: recent advances, challenges, and future perspectives. *Energy Environ Sci.* 2017;10(10):2056-2080.
- Chen X, Liu B, Zhong C, et al. Ultrathin Co<sub>3</sub>O<sub>4</sub> layers with large contact area on carbon fibers as high-performance electrode for flexible zinc-air battery integrated with flexible display. *Adv Energy Mater.* 2017;7(18):1700779.
- Wang H-F, Tang C, Zhang Q. A review of precious-metal-free bifunctional oxygen electrocatalysts: rational design and applications in Zn-air batteries. *Adv Funct Mater.* 2018;28(46):1803329.
- Yu J, Li BQ, Zhao CX, Liu JN, Zhang Q. Asymmetric air cathode design for enhanced interfacial electrocatalytic reactions in high-performance zinc-air batteries. *Adv Mater.* 2020; 32:1908488.
- Fu J, Cano ZP, Park MG, Yu A, Fowler M, Chen Z. Electrically rechargeable zinc-air batteries: progress, challenges, and perspectives. *Adv Mater.* 2017;29(7):1604685.
- Niu W, Pakhira S, Marcus K, Li Z, Mendoza-Cortes JL, Yang Y. Apically dominant mechanism for improving catalytic activities of N-doped carbon nanotube arrays in rechargeable zinc-air battery. *Adv Energy Mater.* 2018;8(20):1800480.
- Tan P, Chen B, Xu H, et al. Co<sub>3</sub>O<sub>4</sub> nanosheets as active material for hybrid Zn batteries. *Small.* 2018;14(21):1800225.
- Zhong Y, Pan Z, Wang X, et al. Hierarchical Co<sub>3</sub>O<sub>4</sub> nano-micro arrays featuring superior activity as cathode in a flexible and rechargeable zinc-air battery. *Adv Sci.* 2019;6(11):1802243.
- Liu Q, Wang Y, Dai L, Yao J. Scalable fabrication of nanoporous carbon fiber films as bifunctional catalytic electrodes for flexible Zn-air batteries. *Adv Mater.* 2016;28(15):3000-3006.
- Guan C, Sumboja A, Zang W, et al. Decorating Co/CoN<sub>x</sub> nanoparticles in nitrogen-doped carbon nanoarrays for flexible and rechargeable zinc-air batteries. *Energy Storage Mater.* 2019; 16:243-250.
- Liu W, Ren B, Zhang W, et al. Defect-enriched nitrogen doped-graphene quantum dots engineered NiCo<sub>2</sub>S<sub>4</sub> nanoarray as high-efficiency bifunctional catalyst for flexible Zn-air battery. *Small.* 2019;15(44):1903610.
- Zhang J, Zhao Z, Xia Z, Dai L. A metal-free bifunctional electrocatalyst for oxygen reduction and oxygen evolution reactions. *Nature Nanotech.* 2015;10(5):444-452.
- Zhang J, Qu L, Shi G, Liu J, Chen J, Dai L. N,P-codoped carbon networks as efficient metal-free bifunctional catalysts for oxygen reduction and hydrogen evolution reactions. *Angew Chem Int Ed.* 2016;55(6):2230-2234.
- Pei Z, Li H, Huang Y, et al. Texturing in situ: N, S-enriched hierarchically porous carbon as a highly active reversible oxygen electrocatalyst. *Energy Environ Sci.* 2017;10(3):742-749.
- Cai X, Xia BY, Franklin J, et al. Free-standing vertically-aligned nitrogen-doped carbon nanotube arrays/graphene as air-breathing electrodes for rechargeable zinc-air batteries. *J Mater Chem A.* 2017;5(6):2488-2495.
- Kordek K, Jiang L, Fan K, et al. Two-step activated carbon cloth with oxygen-rich functional groups as a high-performance additive-free air electrode for flexible zinc-air batteries. *Adv Energy Mater.* 2019;9(4):1802936.
- Zhao Z, Yuan Z, Fang Z, et al. In situ activating strategy to significantly boost oxygen electrocatalysis of commercial carbon cloth for flexible and rechargeable Zn-air batteries. *Adv Sci.* 2018;5(12):1800760.
- Su C-Y, Cheng H, Li W, et al. Atomic modulation of FeCo-nitrogen-carbon bifunctional oxygen electrodes for rechargeable and flexible all-solid-state zinc-air battery. *Adv Energy Mater.* 2017;7(13):1602420.

28. Tang C, Wang B, Wang HF, Zhang Q. Defect engineering toward atomic Co-N<sub>x</sub>-C in hierarchical graphene for rechargeable flexible solid Zn-air batteries. *Adv Mater*. 2017;29(37):1703185.
29. Jiang H, Liu Y, Li W, Li J. Co Nanoparticles confined in 3D nitrogen-doped porous carbon foams as bifunctional electrocatalysts for long-life rechargeable Zn-air batteries. *Small*. 2018;14(13):1703739.
30. Zhao X, Abbas SC, Huang Y, Lv J, Wu M, Wang Y. Robust and highly active FeNi@NCNT nanowire arrays as integrated air electrode for flexible solid-state rechargeable Zn-air batteries. *Adv Mater Interfaces*. 2018;5(9):1701448.
31. Lu Q, Zhong Y, Zhou W, Liao K, Shao Z. Dodecylamine-induced synthesis of a nitrogen-doped carbon comb for advanced lithium-sulfur battery Cathodes. *Adv Mater Interfaces*. 2018;5(9):1701659.
32. Sun Z, Wang X, Zhao H, et al. Rambutan-like hollow carbon spheres decorated with vacancy-rich nickel oxide for energy conversion and storage. *Carbon Energy*. 2020;2(1):122-130.
33. Guo Z, Wang F, Xia Y, et al. In situ encapsulation of core-shell structured Co@Co<sub>3</sub>O<sub>4</sub> into nitrogen-doped carbon polyhedra as a bifunctional catalyst for rechargeable Zn-air batteries. *J Mater Chem A*. 2018;6(4):1443-1453.
34. Zang W, Sumboja A, Ma Y, et al. Single Co atoms anchored in porous N-doped carbon for efficient zinc-air battery cathodes. *ACS Catal*. 2018;8(10):8961-8969.
35. Zhang C, Lv W, Zhang W, et al. Reduction of graphene oxide by hydrogen sulfide: a promising strategy for pollutant control and as an electrode for Li-S batteries. *Adv Energy Mater*. 2014;4(7):1301565.
36. Qiu H, Cheng H, Meng J, Wu G, Chen S. Magnetothermal microfluidic-assisted hierarchical microfibers for ultrahigh-energy-density supercapacitors. *Angew Chem Int Ed*. 2020:2000951.
37. Cui H, Jiao M, Chen Y-N, et al. Molten-salt-assisted synthesis of 3D holey N-doped graphene as bifunctional electrocatalysts for rechargeable Zn-air batteries. *Small Methods*. 2018;2(10):1800144.
38. Zhang K, Zhang Y, Zhang Q, et al. Metal-organic framework-derived Fe/Cu-substituted Co nanoparticles embedded in CNTs-grafted carbon polyhedron for Zn-air batteries. *Carbon Energy*. 2020:1-11.
39. Lu Q, Yu J, Zou X, et al. Self-catalyzed growth of Co, N-codoped CNTs on carbon-encased CoS<sub>x</sub> surface: a noble-metal-free bifunctional oxygen electrocatalyst for flexible solid Zn-air batteries. *Adv Funct Mater*. 2019;29(38):1904481.
40. Yang H, Wang B, Li H, et al. Trimetallic sulfide mesoporous nanospheres as superior electrocatalysts for rechargeable Zn-air batteries. *Adv Energy Mater*. 2018;8(34):1801839.
41. Yang J, Liu H, Martens WN, Frost RL. Synthesis and characterization of cobalt hydroxide, cobalt oxyhydroxide, and cobalt oxide nanodiscs. *J Phys Chem C*. 2010;114:111-119.
42. Hu C, Dai L. Carbon-based metal-free catalysts for electrocatalysis beyond the ORR. *Angew Chem Int Ed*. 2016;55:2-25.
43. Li L, Yang H, Miao J, et al. Unraveling oxygen evolution reaction on carbon-based electrocatalysts: effect of oxygen doping on adsorption of oxygenated intermediates. *ACS Energy Lett*. 2017;2(2):294-300.
44. Li Y, Gao J, Zhang F, Qian Q, Liu Y, Zhang G. Hierarchical 3D macrosheets composed of interconnected in situ cobalt catalyzed nitrogen doped carbon nanotubes as superior bifunctional oxygen electrocatalysts for rechargeable Zn-air batteries. *J Mater Chem A*. 2018;6(32):15523-15529.
45. Fu K, Wang Y, Mao L, et al. Strongly coupled Co, N co-doped carbon nanotubes/graphene-like carbon nanosheets as efficient oxygen reduction electrocatalysts for primary zinc-air battery. *Chem Eng J*. 2018;351:94-102.
46. Sumboja A, Lübke M, Wang Y, An T, Zong Y, Liu Z. All-solid-state, foldable, and rechargeable Zn-air batteries based on manganese oxide grown on graphene-coated carbon cloth air cathode. *Adv Energy Mater*. 2017;7(20):1700927.

## SUPPORTING INFORMATION

Additional supporting information may be found online in the Supporting Information section.

**How to cite this article:** Lu Q, Zou X, Liao K, et al. Direct growth of ordered N-doped carbon nanotube arrays on carbon fiber cloth as a free-standing and binder-free air electrode for flexible quasi-solid-state rechargeable Zn-Air batteries. *Carbon Energy*. 2020;2:461-471.  
<https://doi.org/10.1002/cey2.50>